

GLOBAL JOURNAL OF ENGINEERING SCIENCE AND RESEARCHES
ANALYSIS OF THE EFFECT OF Pb^{2+} PRECURSOR CONCENTRATION ON THE
OPTICAL BAND GAP AND URBACH ENERGY OF ANNEALED $CuO/Pb_{1-x}S$ CORE-SHELL
THIN FILMS DEPOSITED BY SOLUTION GROWTH TECHNIQUE

C. Augustine¹, R.A. Chikwenze¹, F.N.C. Anyaegbunam¹, B.J. Robert², E.P. Obot¹ & P.N. Kalu

¹Department of Physics/Geology/Geophysics, Alex Ekwueme Federal University Ndufu Alike Ikwo,
Ebonyi State, Nigeria

²Department of Electrical/Electronics Engineering Technology, Akanu Ibiam Federal Polytechnic,
Unwana, Ebonyi State, Nigeria

ABSTRACT

$CuO/Pb_{1-x}S$ ($x=0.7M, 0.8M$ and $0.9M$) thin films were deposited on microscopic glass substrates by solution growth technique from aqueous solutions of copper sulphate, potassium chloride, lead nitrate, sodium hydroxide and thiourea in which ammonia solution and thiourea were used as complexing agents. The elemental components of Cu, Pb, S and O were quantitatively obtained from RBS analysis. The optical properties were characterized using the absorbance measurement from GENESYS 10S model UV-VIS spectrophotometer at normal incidence of light in the wavelength range of 300-1000 nm from which transmittance, absorption coefficient and band gap were estimated. We report on the effect of Pb^{2+} concentration on some optical properties of the grown films. In particular, the band gap and Urbach energy were analyzed. It was revealed that increasing the precursor concentration increases the band gap from 3.85 eV to 4.00 eV. After annealing, the band gap of 0.1M Pb^{2+} layer increases from 3.85 eV to 4.00eV while the band gap of 0.2M Pb^{2+} and 0.3M Pb^{2+} layers decreases from 3.85 eV-4.00 eV and 3.75 eV-4.00 eV respectively. The Urbach energy exhibited a decreasing trend with respect to the parametric variation of both concentration and post deposition temperature, indicating reduction in structural defects and improvement of the microstructure of the films. The Urbach energy decreases from 3.50 eV - 3.35 eV, 3.50 eV – 3.25 eV, and 3.75-3.40 eV for 0.1M, 0.2M and 0.3 M of Pb^{2+} respectively. The values of the band gaps are in the range suitable for various solar photovoltaic architecture and fabrication of optoelectronic devices.

Keywords: annealing, bandgap, Urbach energy, Pb^{2+} concentration, temperature.

I. INTRODUCTION

Thin film technology is a fast growing field and the number of applications increases every day due to their low production costs. It is indispensable in the fabrication of novel materials for energy conversion and utilization. Materials fabricated from thin film technology are used as protective coatings on tools, as UV-light protections on windows, as diffusion barriers and connectors for all types of micro components in the electronics industry, as electroplated films for decoration and protection [1]. In view of the various applications of thin films, many research groups have explored thin film technology which led to the emergence of several deposition techniques, most of which require steady power supply because they involve high temperature process [2-4]. The solution growth technique is a low temperature process that does not require sophisticated instruments. Hence, a variety of substrates such as insulators, semiconductors or metals can be used, since it is a low temperature process. This technique has been used extensively possibly because it is relatively inexpensive, simple and convenient for large area deposition. Most of the core-shell thin films fabricated via this technique are either oxide/oxide or sulphide/sulphide based. The review of literature showed that research works on sulphide/oxide or oxide/sulphide thin films are few. Presently, none has deposited ternary $CuO/Pb_{1-x}S$ core-shell thin film using the solution growth technique. However, many binary thin films of CuO and PbS have been deposited using this technique [5-10].

Copper oxide (CuO) thin film has a direct band gap of 2.0eV [11], while lead sulphide (PbS) has direct band gap of 0.40eV [12]. Integrating these binary films to form a new ternary $CuO/Pb_{1-x}S$ thin film has the potential of tailoring the band gap for special applications. This assertion can easily be investigated by making use of spectrophotometer

to measure the absorbance from which transmittance, reflectance, absorption coefficient, band gap and other optical parameters can be determined. Many studies on core-shell thin films to investigate the variation of these parameters with annealing temperature have been reported [13-20]. However, few reports are available on the effect of concentration on the properties of core-shell thin films. In this article, we report on the effect of Pb^{2+} precursor concentration on the band gap and Urbach energy of $CuO/Pb_{1-x}S$ core-shell thin films.

II. THEORETICAL CONSIDERATIONS

Optical characterization of thin films require accurate knowledge of the optical constants over a wide wavelength range. Most spectrophotometer give the absorbance data from which transmittance and other optical constants are determined. The transmittance (T), reflectance (R), absorption coefficient (α), band gap (E_g), refractive index (n), extinction coefficient (k), real (ϵ_r) and imaginary (ϵ_i) dielectric constants are usually calculated using relevant equations available in literature [21-23]. The transmittance can be calculated using equation (1)

$$T = (1 - R^2) \exp(-A) \quad (1)$$

The reflectance is related to absorbance and transmittance as expressed in the equation below.

$$R = 1 - [T \exp(A)]^{\frac{1}{2}} \quad (2)$$

The absorption coefficient, α is related to absorbance and thickness, t of thin film:

$$\alpha = \frac{2.3026 \times A}{t} \quad (3)$$

The band gap is determined from Tauc's relation as:

$$(\alpha h\nu) = B(h\nu - E_g)^n \quad (4)$$

Where in equation 4, α is the optical absorption coefficient, B is an energy independent constant but depends on the refractive index and the effective masses of the hole and electron respectively [24], E_g is the energy band gap, and n is an index that characterises the nature of the transition. For $n = 1/2$, the transition is generally accepted to be direct. According to the literature [25, 26], B is given by the equation;

$$B \approx \frac{q^2 \left[2 \frac{M_h^* M_e^*}{M_h^* + M_e^*} \right]^{\frac{3}{2}}}{nch^2 M_e^*} \quad (5)$$

where q is the electronic charge, n is the refractive index, c is the speed of light in free space, h is the Planck's constant, m_e and m_h are the effective masses of the electrons and holes respectively. It has been established [27] that for $n = 4$, and suppose the hole and electron effective masses are equal to the free electron mass, equation 5 will reduce to;

$$(\alpha h\nu) = 2 \times 10^4 (h\nu - E_g)^n \text{ cm}^{-1} \quad (6)$$

Where $h\nu$ and E_g are expressed in electron volts. It is a common knowledge that extrapolation of the plots of

$(\alpha h\nu)^2$ vs $h\nu$ down the photon energy axis usually give the energy band gap.

III. EXPERIMENTAL

Glass microscope slides were cleaned by degreasing them in dilute hydrochloric acid for 24 hours, washed in detergent solution, rinsed in distilled water and dried in air. In a typical deposition set up, the bath was composed of 4mls of 1M $CuSO_4$, 4mls of KCl, 2mls of 10M NH_3 solution and 13mls of distilled water put in that order. The clean

substrate was inserted vertically into the solution with the use of synthetic foam. The deposition lasted for 3 hours in the oven set at 80°C. After the expiration of 3 hours, the coated substrates were removed, washed well with distilled water and allowed to dry. The substrates coated with CuO deposits were inserted into a chemical bath composed 5mls of 0.1M-0.3M $Pb(NO_3)_2$, 5mls of 1M SC $(NH_2)_2$, 5mls of 1M NaOH and 35mls of distilled water put in that order in 50ml beaker for 50 minutes. This enabled the formation of CuO/ $Pb_{1-x}S$ composites. A total of three experimental set-ups were prepared with different concentration of Pb^{2+} precursor, and labelled A1 (0.1M $Pb(NO_3)_2$), A2 (0.2M $Pb(NO_3)_2$) and A3 (0.3M $Pb(NO_3)_2$). The deposited films were subjected to thermal annealing in an oven at 200°C and 400°C for 1 hour.

The optical absorption data were obtained with a thermo scientific GENESYS 10S model UV-VIS spectrophotometer at normal incidence of light in the wavelength range of 300-1000 nm from which other optical and solid state properties of the film were estimated. Proton Induced X-ray Emission (PIXE) scans were done on the samples from a Tandem Accelerator Model 55DH 1.7MV Pellaton by National Electrostatic Corporation (NEC), USA which effectively performed Rutherford Back Scattering (RBS) elemental characterizations on both deposits and substrates. The RBS also deciphered the thicknesses of deposits as well as substrates. The surface morphology of the films was taken by scanning electron microscope (Tescan model).

IV. RESULTS and DISCUSSION

Typical XRD diffractogram of CuO/ $Pb_{1-x}S$ thin films at 0.2M Pb^{2+} concentration is presented in fig. 1. The samples were loaded into Rigaku Ultima IV X-ray diffractometer equipped with a graphite-monochromated CuK_{α} radiation source (40KV, 30mA), the peak at 2θ value of 35.583° corresponding to (212) plane is attributed to copper hydroxide sulphate phase which is in good agreement with Joint Committee on Powder Diffraction Standard (JCPDS) data cards (JCPDS 00-011-0653). The growth of anglesite lead oxide sulphate phase $PbSO_4$ (JCPDS 00-036-1461) at 2θ values of 29.680° and 44.546° corresponding to (121) and (231) reflections was also revealed.

The dependence of grain size on annealing temperature is demonstrated in Fig.2, a plot of grain size as a function of temperature for CuO/ $Pb_{1-x}S$ thin films. The grain size increased rapidly with increase in annealing temperature from 19.14nm to 29.44nm. The dislocation density and micro strain were observed to decrease with increasing annealing temperature (Fig.3).

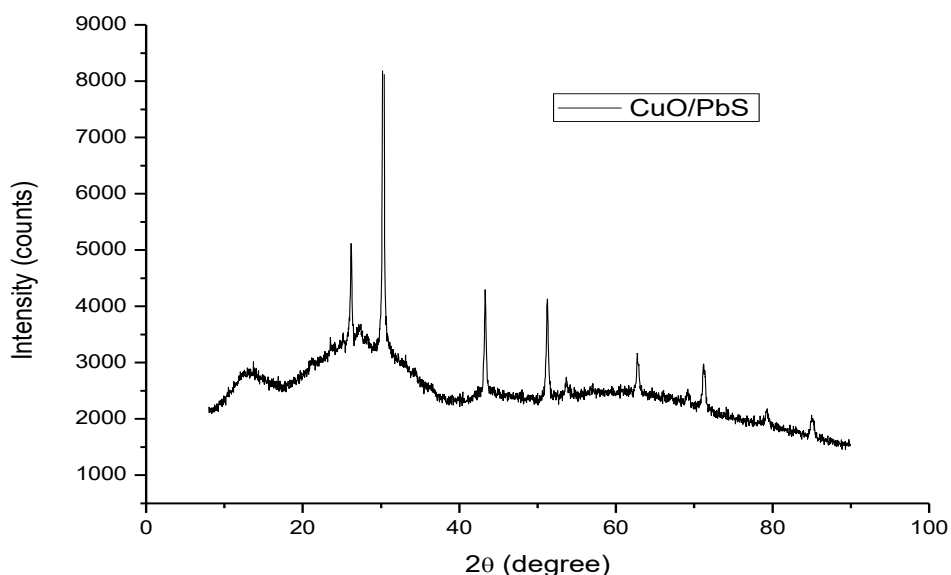


Fig.1: XRD diffractogram of CuO/ $Pb_{1-x}S$ thin films

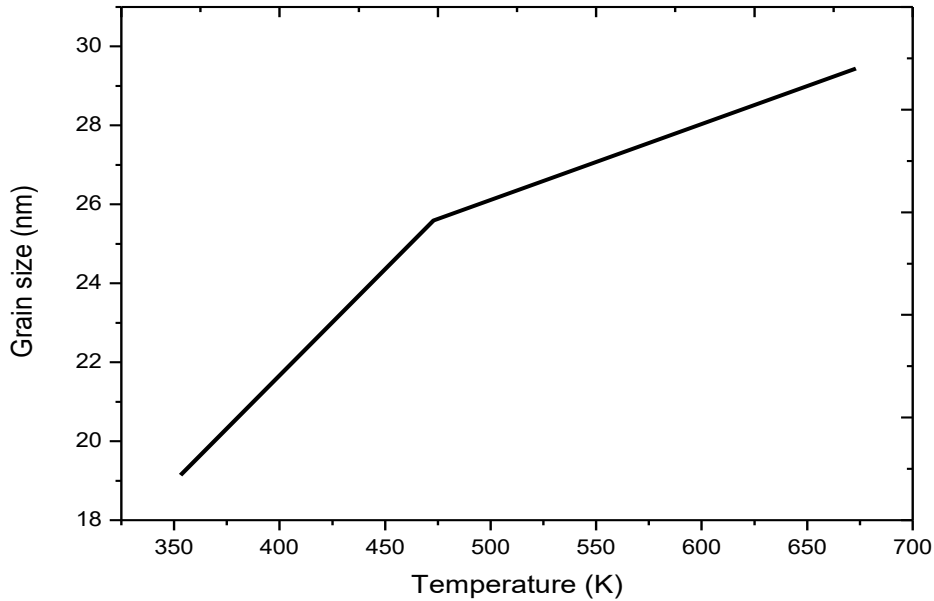


Fig.2: Plot of grain size against temperature of CuO/Pb_{1-x}S thin films

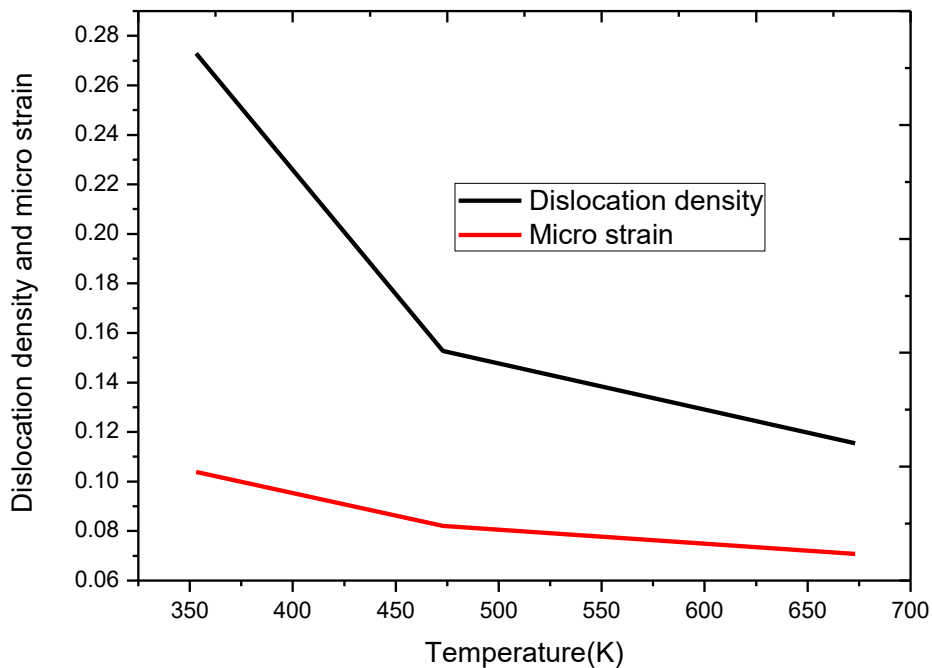


Fig.3: Plots of dislocation density and micro strain against temperature of CuO/Pb_{1-x}S thin films

The elemental composition and chemical state of the films at 0.2M Pb²⁺ concentration was analysed by Rutherford Backscattering (RBS). The result is presented in fig. 4. From the film composition, we can deduce that CuO/Pb_{1-x}S

thin film consists of 5.64% of copper (Cu), 94.36% of oxygen (O), Pb (5.00%) and 33.16% of sulphur (S). This is an indication that CuO/Pb_{1-x}S thin films were actually deposited on the glass substrates. Other elements such as calcium, potassium, sodium etc may have come from the glass substrates.

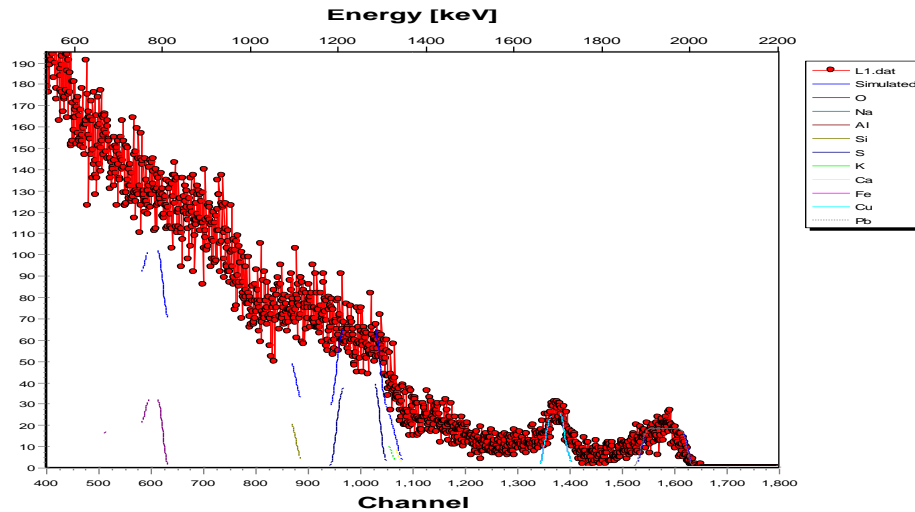


Fig. 4: RBS result for CuO/PbS thin films for as-deposited

Thickness of films is a very important parameter. Apart being used to classify films into thick or thin, the thickness of films influences the properties. The thickness of 0.2M sample of CuO/Pb_{1-x}S thin films as deciphered by RBS analysis is 650nm. The resistance for a thin film layer (thickness $t \ll s$), in which current rings exist instead of spheres is derived as follows:

$$R = \int_{x_2}^{x_1} \rho \frac{dx}{2\pi xt} = \int_s^{2s} \frac{dx}{2xtx} = \frac{\rho}{2\pi xt} \ln(x) \int_s^{x_2} dx = \frac{\rho}{2\pi t} \ln 2 \quad (7)$$

Consequently, for $R = \frac{V}{2I}$, the sheet resistivity for a thin sheet is:

$$R = \frac{\pi t}{\ln 2} \left(\frac{V}{I} \right) \quad (8)$$

This expression is independent of the probe spacing and frequently used for characterization of semiconductor layers. In general, the sheet resistivity R_s can be expressed as [28]:

$$R_s = k \left(\frac{V}{I} \right) \quad (9)$$

Where the factor k is a geometric factor. In the case of semi-infinite thin sheet, $k=4.53$ which is just $\frac{\pi}{\ln 2}$ from the derivation. The factor k will be different for non-ideal samples. V/I in equation (10) is equal to the resistance of the thin film samples.

Where V is the measured voltage between the two inner probes and I is the current passed through the outer probes. The resistance of the film samples was measured by a four point probe (Keithley model). The resistivity was determined from the relation [29]:

$$\rho = R_s t \quad (10)$$

Where t is the thickness of the conducting layer while ρ is the resistivity and R_s is the sheet resistance. From the value of ρ , the conductivity σ was determined using the relation [29]:

$$\sigma = \frac{1}{\rho} \quad (11)$$

Table 1 shows the summary of the electrical properties of the film samples at different annealing temperatures. Post deposition annealing has profound effect on the electrical properties of the films as indicated in the table 1. All the electrical properties decreases with temperature with the exception of the conductivity which is the reverse. This behaviour clearly shows the semiconducting nature of the films. With respect to grain size, increasing the annealing temperature from 473K to 673K, will enhance the formation of fine and large grains. This increase in the grain size leads to a decrease in the density of the grain boundaries which is due to the improvement of crystallinity and film orientation leading to a reduction in the donor sites that are trapped at the dislocations and grain boundaries. As a result, there is enhancement in the carrier concentration due to decrease in resistivity leading to increase in conductivity. Similar phenomenon has been reported by other research groups [30, 31]. The electrical conductivity, dislocation density and micro strain were found to be directly related in all samples. As such the film annealed at 673K, which is less strained and having minimum dislocation density shows maximum electrical conductivity.

Table 1: Summary of electrical properties of CuO/Pb_{1-x}S thin films

Sample	Sheet resistance (Ω)	Resistivity(Ωm)	Conductivity($\Omega^{-1}\text{m}^{-1}$)
As-deposited	1.3952	9.0688	0.1102
473K	0.1296	0.6091	1.6418
673K	0.1023	0.4932	2.0276

Fig. 5 gives the absorbance versus wavelength λ spectra for the as-deposited layers while Figs. 6 and 7 show the absorbance versus wavelength λ plots for the layers annealed at 200°C and 400°C respectively for 1 hour.

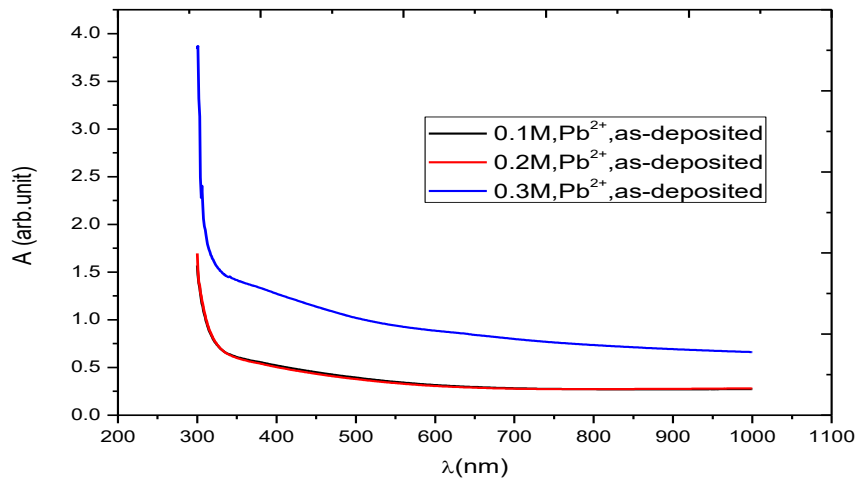


Fig.5: Plots of absorbance (A) against wavelength (λ) as-deposited

As indicated in the experimental section, the optical absorption data were obtained with a thermo scientific GENESYS 10S model UV-VIS spectrophotometer at normal incidence of light in the wavelength range of 300-1000 nm from which other optical and solid state properties of the film were estimated. From Fig.5, it was observed that the film deposited with 0.3M of Pb²⁺ has the highest value of absorbance of about 3.83 (arb.unit) followed by film deposited with 0.2M of Pb²⁺ while the film deposited with 0.1 M of Pb²⁺ recorded the lowest value of absorbance.

Post deposition temperature clearly influenced the absorbance of the film samples at different Pb^{2+} concentration as observed in figs. 6 to 7. After annealing at $200^{\circ}C$, the absorbance of $0.3M Pb^{2+}$ concentration increased to 4.00 (arb.unit) with significant increases noticed for $0.2M$ and $0.1M Pb^{2+}$ concentrations. The absorbance increased from 1.60 to 2.03 (arb.unit) for $0.1M$ and 1.70 to 3.47 (arb.unit) at $0.2M$. However, the film annealed at $400^{\circ}C$ showed no trend with post deposition temperature at different Pb^{2+} concentration. Here, $0.2M$ depicts highest absorbance followed by $0.3M$ with $0.1M$ exhibiting minimum absorbance. It is observed that at higher annealing temperature, the absorbance of $0.1M$ and $0.3M$ layers significantly reduced. Generally, the absorbance is higher in the ultraviolet region exhibiting minimum in the infrared region. Our absorbance values are in the same order of magnitude with the values reported elsewhere [14-17]. The high absorbance displayed by the films could be used as spectrally selective coating for solar thermal applications. This is predicated on the fact that solar collectors for heating fluids require increasing the reception area of the solar radiation, and/or to increase the absorbance of the surface coating in order to improve thermal efficiency[32].

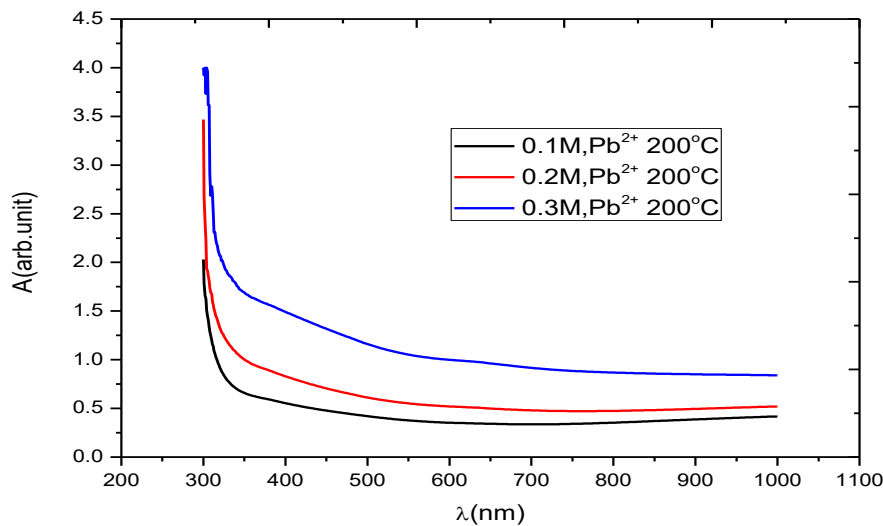


Fig.6: Plots of absorbance (A) against wavelength (λ) annealed at $200^{\circ}C$

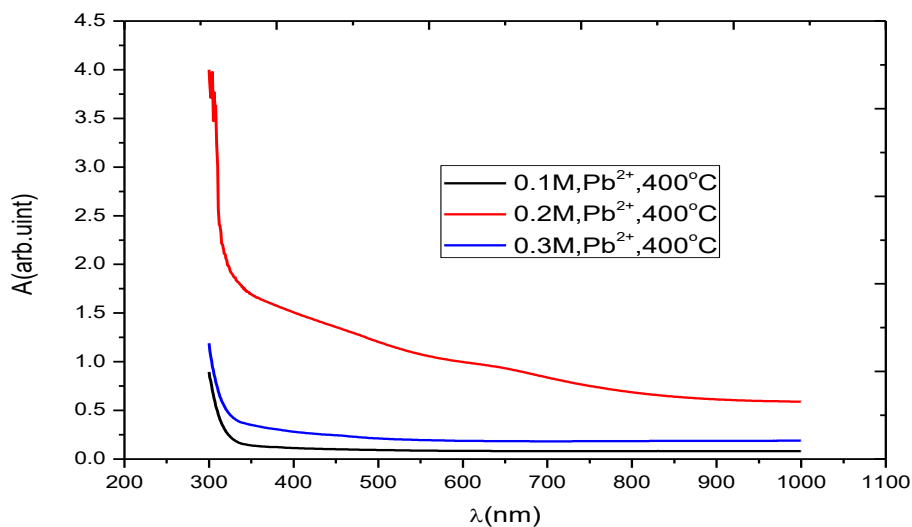


Fig.7: Plots of absorbance (A) against wavelength (λ) annealed at $400^{\circ}C$

The variation of transmittance against wavelength for as-deposited film samples at different Pb^{2+} concentration is shown in fig.8 while figures 9 and 10 depict the transmission spectra of the deposited films annealed at 200°C and 400°C respectively. Table 2 gives the values of the transmittance of the film samples for as-deposited at different Pb^{2+} concentration at some specific wavelength while that of the annealed at 200°C and 400°C are shown in tables 3 and 4 respectively. From table 2, it was observed that the transparency of $CuO/Pb_{1-x}S$ films varies from 30.13-52.24% in the visible region and 53.33-53.46% in the infrared region at 0.1M Pb^{2+} concentration. Similar trend was observed for the films deposited at 0.2M Pb^{2+} . However, at 0.3M Pb^{2+} , the transparency reduced significantly. The reduction in the transmittance with increase in Pb^{2+} concentration is based on the fact that at higher concentration, the constituent atoms will be more and more, as well as the light particle collisions with atoms resulting to low transmission of light [33-35]. It should be noted that when the concentration is high, the ions in solution would be high as well, leading to high rate of film formation. As such thicker films are grown at higher metallic precursor concentration.

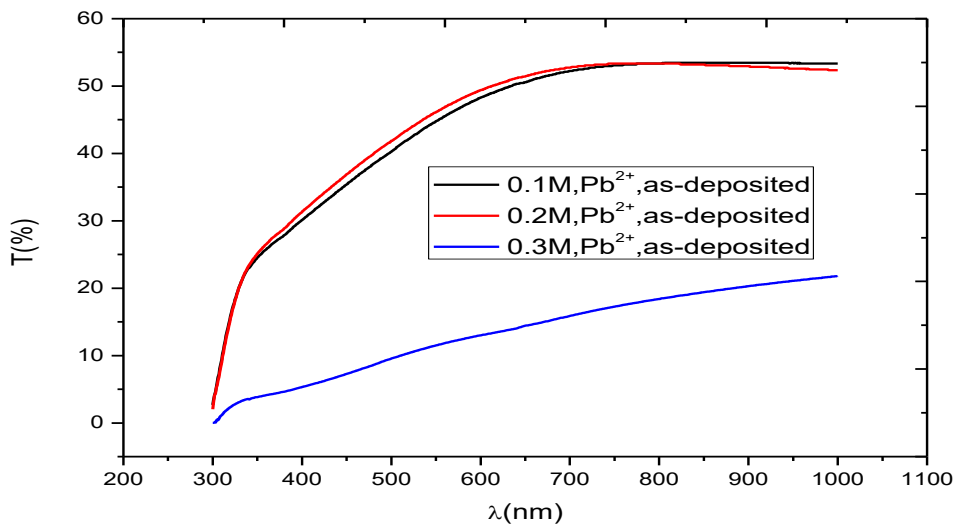


Fig.8: Plots of transmittance (T) against wavelength (λ) for as-deposited

Table 2: Percentage transmittance of $CuO/Pb_{1-x}S$ at different Pb^{2+} concentration for as-deposited

Sample	300 nm	400 nm	500 nm	600 nm	700 nm	800 nm	900 nm	1000 nm
0.1M	2.69	30.13	40.27	48.31	52.24	53.33	53.46	53.33
0.2M	2.02	31.33	41.88	49.43	52.72	53.33	52.97	52.36
0.3M	0.01	5.33	9.55	13.00	15.89	18.41	20.28	21.83

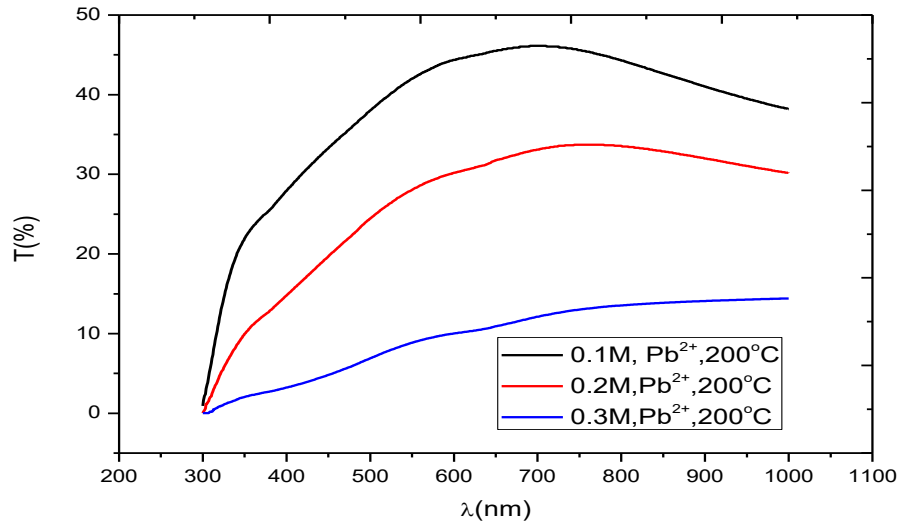


Fig.9: Plots of transmittance (T) against wavelength (λ) for annealed at 200°C

After annealing at 200°C, the transparency of the films decreased at different Pb²⁺ concentration exhibiting minimum for the 0.3M layer. Further post deposition annealing at 400°C significantly improved the transparency of the filmsexhibiting a minimum for 0.2M Pb²⁺. Table 3 show that at 0.1M, the transparency increased from 77.09 to 82.79% in the visible region, 82.79.82.99% in the near infrared region. For 0.2M, it varies in the range 3.11-20.60% in the visible region, 20.60-25.70% in the infrared region.

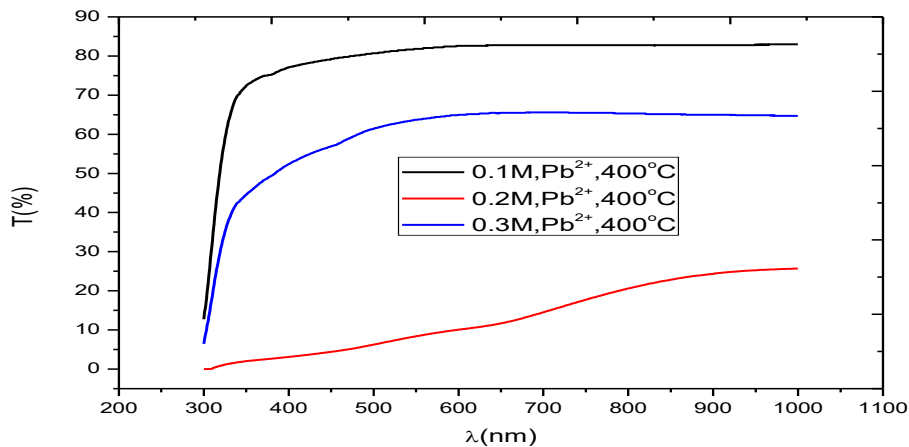


Fig.10: Plots of transmittance (T) against wavelength (λ) annealed at 400°C

The variation of transmittance for 0.3M layer shows that it varies from 52.36-65.31% in the visible region to 64.71-65.31% in the infrared region. Generally, all films both the as-deposited and annealed layers showed higher transparency in the infrared region with optimum transparency observed for the films annealed at 400°C at different Pb²⁺ concentration. The infrared region is generally known as the heat region. Based on the property of high transmittance in the NIR exhibited by the films, the films can be used for the construction of poultry roofs and walls to provide source of heat in chick brooding. This has the potential to minimize the cost of energy consumption

associated with the use of electric bulbs, heater, stove etc as well as the hazards associated with them. The low transmittance in the UV region will protect the chicks from harmful UV radiation. These findings are in agreement with the report of other authors [36-38].

Table 3: Percentage transmittance of CuO/Pb_{1-x}S films at different Pb²⁺ concentration annealed at 200°C

Sample	300 nm	400 nm	500 nm	600 nm	700 nm	800 nm	900 nm	1000 nm
0.1M	0.93	27.93	38.02	44.36	46.13	44.26	41.02	38.19
0.2M	0.03	14.79	24.43	30.19	33.11	33.57	31.99	30.13
0.3M	0.01	3.23	6.90	10.02	12.11	13.55	14.09	14.42

Table 4: Percentage transmittance of CuO/Pb_{1-x}S films at different Pb²⁺ concentration annealed at 400°C

Sample	300 nm	400 nm	500 nm	600 nm	700 nm	800 nm	900 nm	1000 nm
0.1M	12.71	77.09	80.72	82.60	82.79	82.79	82.79	82.99
0.2M	0.01	3.11	6.25	10.07	20.60	20.60	24.38	25.70
0.3M	6.46	52.36	61.38	65.01	65.31	65.31	64.71	65.01

The absorption spectra, which are the most direct and perhaps the simplest method for probing the band structure of semiconductors, are employed in the determination of the energy gap, E_g. The E_g was calculated using the following Tauc's relation in equation (4) while the absorption coefficient, α was calculated using equation (3). Fig. 11 shows the plots of absorption coefficient as a function of photon energy for the as-deposited at different Pb²⁺ concentration. Accordingly, the film deposited at 0.3M Pb²⁺ has higher values of absorption coefficient. This could be attributed to the thickness of 0.3M layer in which most of the light was absorbed according to Lambert-Beer's law. Figs. 12 and 13 show the plots of α as a function of hv for annealed at 200°C and 400°C respectively, at different Pb²⁺ concentration.

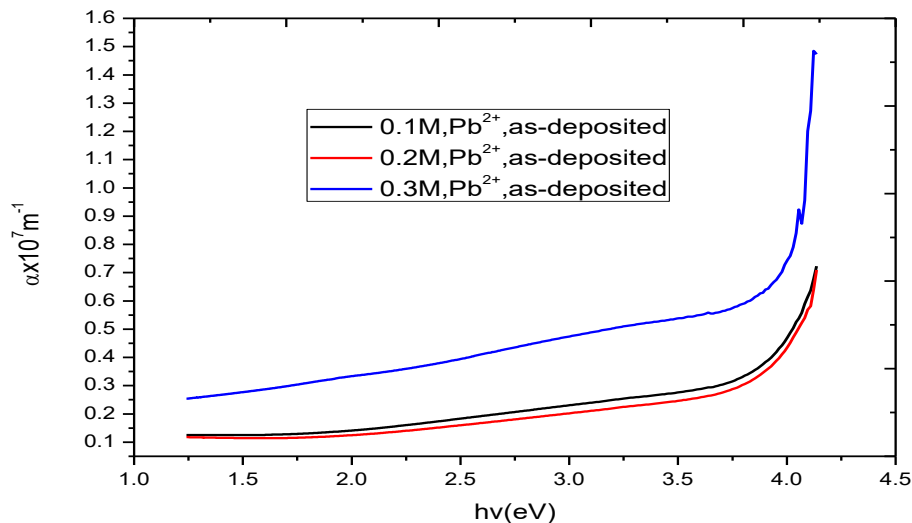


Fig.11: Plots of α against hv for as-deposited at different Pb²⁺ concentration

After post deposition annealing, the values of absorption coefficient of the as-deposited layers at different Pb²⁺ were significantly altered as seen in figs. 12 and 13.

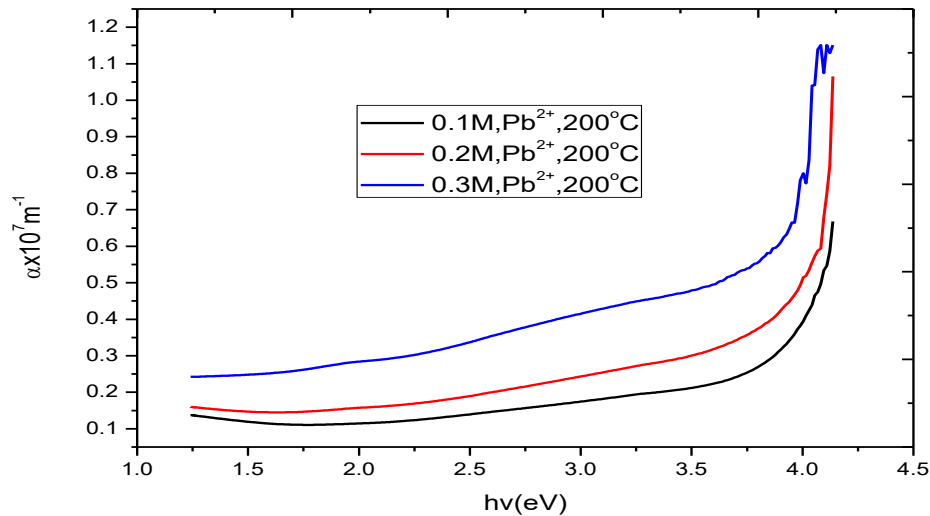


Fig.12: Plots of α against $h\nu$ for annealed at 200°C at different Pb^{2+} concentration

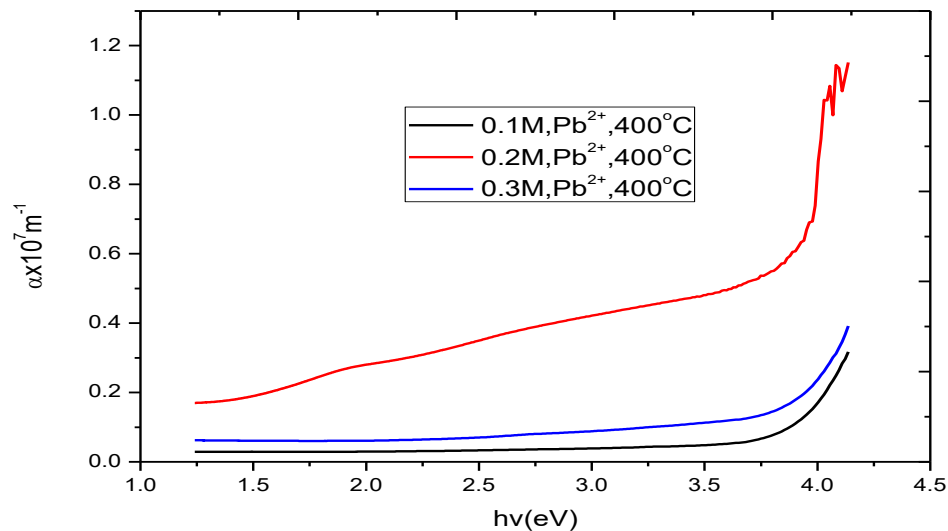


Fig.13: Plots of α against $h\nu$ for annealed at 400°C at different Pb^{2+} concentration

Figs. 14– 16 show the plots for the determination of the optical bandgap. The energy bandgaps were obtained by extrapolating the straight line portions of the $(\alpha h\nu)^2$ versus $h\nu$ to zero absorption coefficients. It is evident from the Table 5-7 and Figures 14-16 that increasing the concentration of the principal precursor increases the band gap. However, the range of bandgaps for the different concentration of Pb^{2+} and post deposition temperature are 3.85 eV – 4.00 eV for 0.1M, 3.85 eV – 4.00 eV for 0.2M and 3.75-4.00 eV for 0.3 M of Pb^{2+} . Post deposition temperature increases the band gap for 0.1M Pb^{2+} , decreases the band gap for 0.2M Pb^{2+} and 0.3M Pb^{2+} . The increase in band gap with increase in the precursor concentration reported in this work is in agreement with the report of other research groups [39]. The successive increase in the bandgap of 0.1M Pb^{2+} as the annealing temperature increases is

in agreement with the report of other authors [40-42]. The decrease in band gap with annealing temperature of 0.2M Pb^{2+} could attributed to quantum size effect [43-45]. The clear variation of E_g of the films with parameters of growth indicates that we can tune the solid state properties of films to suite a desired application. The high transparency in the visible region and wide direct band gap energy exhibited by these films make them ideal for use as window layer in a heterojunction solar cells. The use of wide band gap materials as window layers in solar cell fabrications is to minimize the recombination loss prevalent in direct band gap semiconductors thereby admitting a maximum amount of light to the junction region and the absorber layer. CdS thin films are widely used as window layer in CIGS solar cells. However, there are great concern about the toxicity of Cd in this architecture [46] and so; several alternative window layers are currently being investigated to replace CdS. In our view, $Zn_{1-x}O$ and $Co_{1-x}O$ films stand high for possible incorporation in CIGS solar cell.

Table 5: Variation of E_g, E_u with 0.1M Pb^{2+} conc. and post deposition temperature

Concentration (M)	Post deposition temperature (°C)	E_g (eV)	E_u (eV)
0.1	-	3.85	3.50
0.1	200	3.95	3.40
0.1	400	4.00	3.35

Table 6: Variation of E_g, E_u with 0.2M Pb^{2+} conc. and post deposition temperature

Concentration (M)	Post deposition temperature (°C)	E_g (eV)	E_u (eV)
0.2	-	4.00	3.50
0.2	200	3.98	3.45
0.2	400	3.85	3.25

Table 7: Variation of E_g, E_u with 0.3M Pb^{2+} conc. and post deposition temperature

Concentration (M)	Post deposition temperature (°C)	E_g (eV)	E_u (eV)
0.3	-	4.00	3.75
0.3	200	3.85	3.60
0.3	400	3.75	3.40

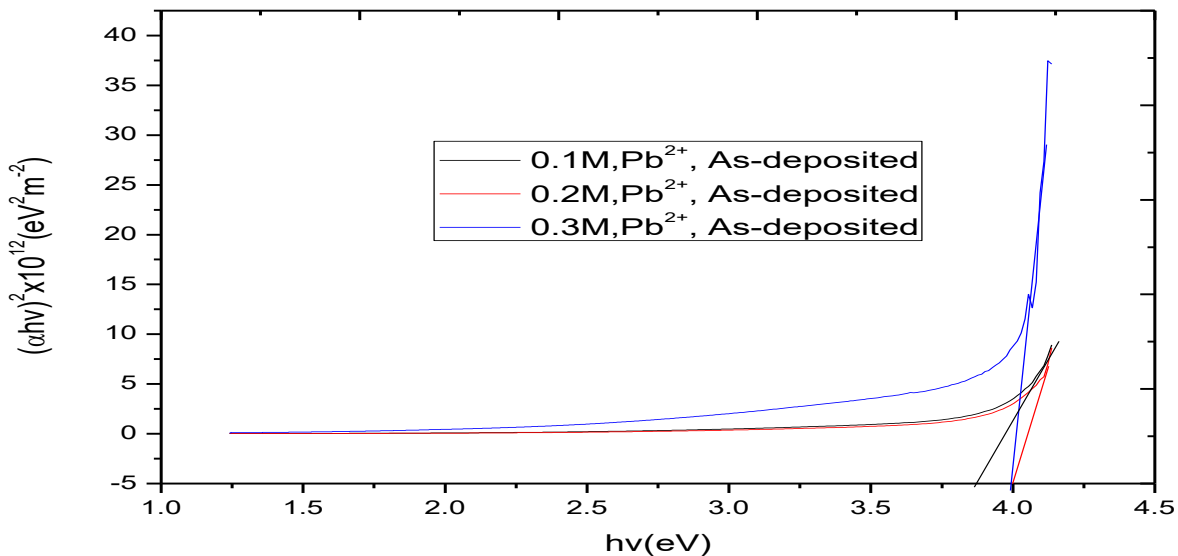


Fig.14: Plots of $(\alpha hv)^2$ against hv for as-deposited at different Pb^{2+} concentration

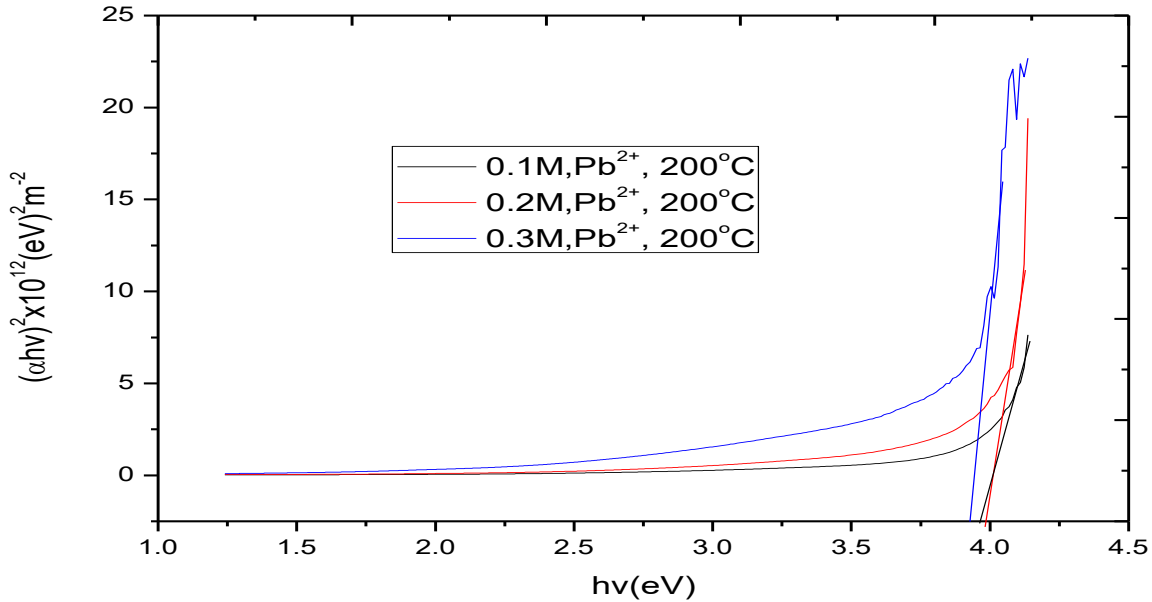


Fig.15: Plots of $(\alpha hv)^2$ against $h\nu$ for annealed at 200°C at different Pb^{2+} concentration

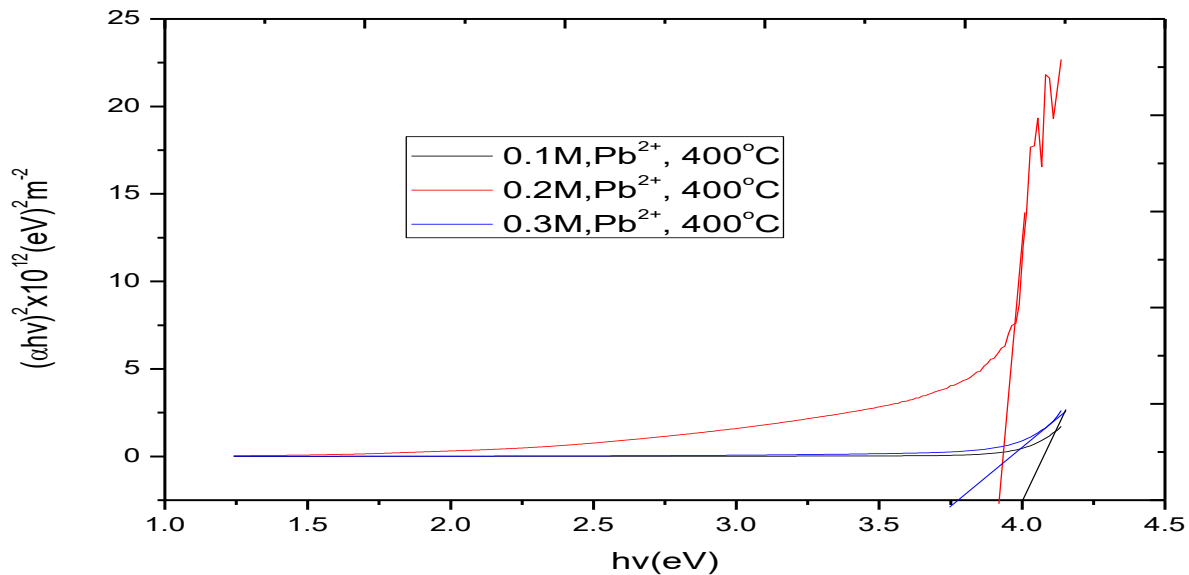


Fig.16: Plots of $(\alpha hv)^2$ against $h\nu$ for annealed at 400°C at different Pb^{2+} concentration

To determine the Urbach energy (E_u), the graph of the natural logarithm of absorption coefficient as a function of photon energy at Pb^{2+} concentrations and post deposition temperatures was plotted and shown in figs. 17-19. The plots depict a decreasing values of E_u at different Pb^{2+} concentration and post deposition temperature indicating an

improvement in the microstructure of the films with annealing temperature. The determination of E_u is based on the empirical rule proposed by [47, 48].

$$\alpha = \alpha_o \exp\left(\frac{hv}{E_u}\right) \tag{12}$$

Where α_o is a constant, E_u denotes an energy which is constant or weakly dependent on temperature and is often interpreted as the width of the tail of localized states in the band gap. The exponential tail appears because disordered and amorphous materials produce localized states extended in the band gap [49]. Taking the logarithm of the two sides of equation (12), gives a straight line equation as expressed in equation (13).

$$\ln \alpha = \ln \alpha_o + \left(\frac{hv}{E_u}\right) \tag{13}$$

Therefore, the band tail energy or urbach energy (E_u) can be obtained from the slope of the straight line of plotting $\ln(\alpha)$ against the incident photon energy (hv). The successive decrease in the band tail or urbach energy is in agreement with the report of [50]. Tables 5-7 show the Urbach energy range for all the film samples.

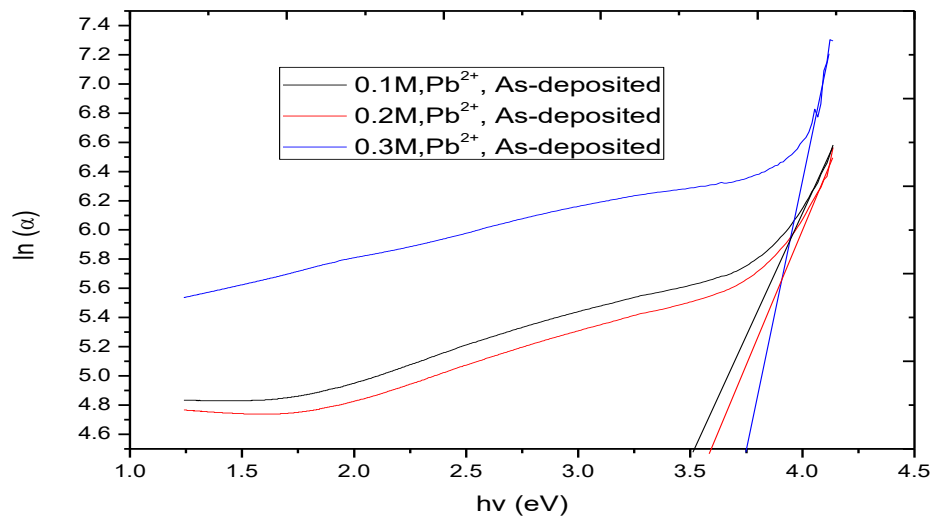


Fig.17: Plots of $\ln(\alpha)$ against hv for as-deposited at different Pb^{2+} concentration

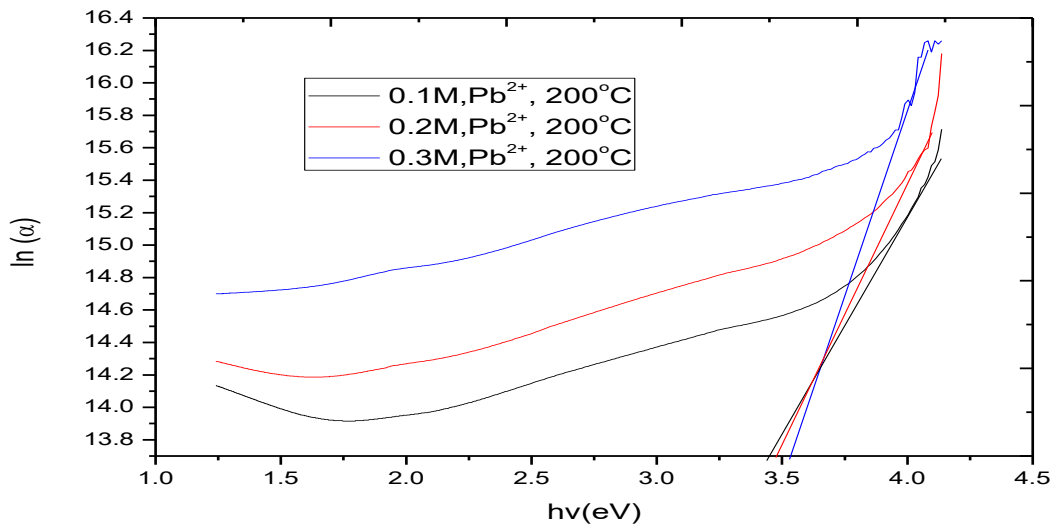


Fig.18: Plots of $\ln(\alpha)$ against $h\nu$ for annealed at 200°C at different Pb^{2+} concentration

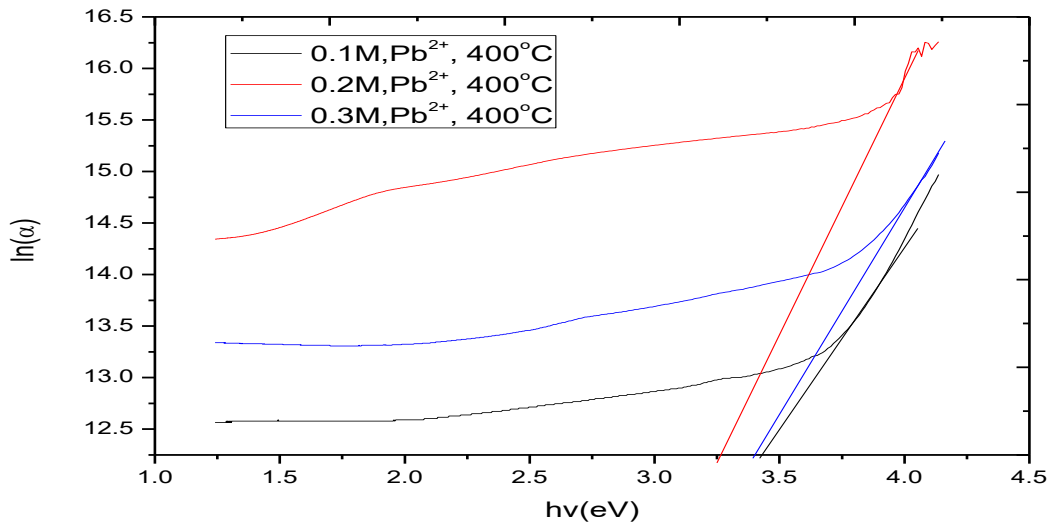


Fig.19: Plots of $\ln(\alpha)$ against $h\nu$ for annealed at 420°C at different Pb^{2+} concentration

V. CONCLUSION

Thin films of $\text{CuO/Pb}_{1-x}\text{S}$ have been successfully deposited on glass substrate by chemical bath deposition technique. The effects of Pb^{2+} concentration on the optical band gap and Urbach energy were investigated. It was revealed that increasing the precursor concentration led to corresponding increase in optical band gap and decrease in Urbach energy. Post deposition temperature showed significant influence on the studied parameters. It resulted to an increase in band gap for 0.1M Pb^{2+} concentration, and decrease in band gap for 0.2M Pb^{2+} and 0.3M Pb^{2+} concentration. The range of bandgaps for the different concentration of Pb^{2+} and post deposition temperature are 3.85 eV – 4.00 eV for 0.1M, 3.85 eV – 4.00 eV for 0.2M and 3.75-4.00 eV for 0.3 M of Pb^{2+} respectively. The

inverse relationship observed between Urbach energy and post deposition temperature indicated an improvement in the microstructure of the films. Based on the properties of the films, they can be applied in optoelectronics, solar cell fabrication, poultry industries etc.

REFERENCES

1. O.S. Heavens, *Thin Film Physics*, Methuen and Co Ltd. London, (1970).
2. L.W. Guo, D.L. Peng, H. Makmo, K. Inaba, H.J. Ko, K. Sumiyama, T. Yao, *J. Magn. Mater.*, **213**, 321 (2000).
3. X.H. Xu, X.F. Qui, F.X. Jang, X.L. Li, Y. Chen, G.A. Gehung, *Appl.Surf.Sci.*, **258**, 4956 (2008).
4. L.O. Oladeji, L. Chow, *Thin Solid Films*, **333**, 148 (1999).
5. C.R. Dhas, D. Alexander, A.J. Christy, K. Jeyadheepan, A.M.E. Raj, C. Raj, *Preparation and characterization of CuO thin films prepared by spray pyrolysis technique for ethanol gas sensing application*, *Asian Journal of Applied Sciences*, **7**(8), 671-684 (2014).
6. F.K. Mugwang, P.K. Karimi, W.K. Njoroge, O. Omayio, S.M. Waita, *Optical characterization of copper oxide thin films prepared by reactive dc magnetron sputtering for solar cell applications*, *Int.J.Thin.Film Sci.Tec.*, **2**(1), 15-24 (2013).
7. R.J. Mohd, S.M.S. Mohd, L.H. Nor, A.C. Hee, *Annealing effects on the properties of copper oxide thin films prepared by chemical deposition*, *Int.J.Electrochem.Sci*, **6**, 6094-6104 (2011).
8. S. Seghaier, N. Kamoun, R. Brini, A.B. Amara, *Structural and optical properties of PbS thin films deposited by chemical bath deposition*, *Materials Chemistry and Physics*, **97**, 71-80 (2006).
9. S. Sakthivel, V. Baskaran, S. Anjali, *Synthesis and characterization of lead sulphide (PbS) thin films by chemical bath deposition (CBD) method*, *International Research Journal of Nano Science and Technology*, **5**(7-9), 248-252 (2015).
10. S. Manouchehri, *Refractive index, optical band gap and oscillator parameter of PbS thin films deposited by CBD technique*, *International Journal of Science and Technology*, **26**(3), 1816-1823 (2014).
11. K. Akimoto, S. Ishizuka, M. Yanagita, Y. Nawa, G.K. Paul, T. Sakurai, *Solar Energy*, *Journal of applied physics*, **80**,715 (2006).
12. J.L. Machol, F.W. Wise, R.C. Patel, D.B. Tanner, *Phys. Rev. B*, **48**, 2819 (1993).
13. P. E. Agbo, M.N. Nnabuchi, *Core-Shell TiO₂/ZnO Thin Film: Preparation, Characterization and effect of temperature on some selected properties*, *Chalcogenide Letters*, **8**(4), 2011, 273-278.
14. C. Augustine, M. N. Nnabuchi, F.N.C. Anyaegbunam, A.N. Nwachukwu, *Study of the effects of thermal annealing on some selected properties of Heterojunction PbS-NiO core-shell thin film*, *Digest Journal of Nanomaterials and Biostructures*, **12**(2), 523-531 (2017)
15. C. Augustine, M.N. Nnabuchi, *Band gap Determination of Novel PbS-NiO-CdO Heterojunction thin film for possible Solar Energy Applications*, *Journal of Ovonic Research*, **13**(4), 233-240 (2017).
16. C. Augustine, M.N. Nnabuchi, *Band gap determination of chemically deposited lead sulphide based heterojunction thin films*, *Journal of Non-Oxide Glasses*, **9**(3), (2017).
17. C. Augustine, M.N. Nnabuchi, *Comparative study of PbS-NiO and NiO-PbS heterojunction thin films deposited by chemical bath deposition technique*, *Chalcogenide Letters*, **15**(12),591-598 (2018).
18. D. U. Onah, C. E. Okeke, F. I. Ezema, A. B. C. Ekwealor, R. U. Osuji, B. A. Ezekoye, *Structural and Optical Properties of Novel core-shell Oxide Materials by Chemical Bath Deposition*. *Journal of Ovonic Research*, **8**(5) 105-111 (2012).
19. P. E. Agbo, M. N. Nnabuchi, D. U. Onah, *TiO₂ /Fe₂O₃ Core-shell Thin Film for Photovoltaic Application*, *Journal of Ovonic Research*, **7** (2) 29-35 (2011).
20. P. E Agbo, G. F. Ibeh, S. O. Okeke, J. E. Epke, *Chemically Deposited Cuprous Oxide Thin Film on Titanium Oxide for Solar Applications*, *Communications in Applied Sciences*, **1**(1) 38-46 (2013).
21. M.C. Tamargo, "Optical Properties of Electronic Structure of Semiconductors," In: C. Hernandez, Ed., *II – VI Semiconductor Materials and Their Application*, Taylor and Francis, New York, 113-170 (2002).
22. C.D. Lokhande, B.R. Sankapal, R.S. Mane, H.M. Pathan, M. Muller, M. Giersig, V. Ganesan *Appl. Surf. Sci.*, **193**, 1 (2002).
23. M. R. Islam, J. Podder, "Optical Properties of ZnO Nano Fibre Thin Films Grown by Spray Pyrolysis of Zinc Acetate Precursor", *Cryst. Res. Technol*, **44**, 286 – 292 (2009).

24. J. Bardeen, F.J. Blatt, L.H. Hall, (1954), *Proc. of Atlantic City Photoconductivity Conference*, J. Wiley and Chapman and Hall (1956).
25. J.I. Pankove, *Optical Processes in Semiconductors*, Prentice-Hall, Englewood Cliffs, New Jersey, 1971.
26. P. A. Nwofe, P.E. Agbo, *Annealing treatments and characterization of nickel-doped antimony sulphide thin films*, *Journal of non-oxide glasses*, **9(1)**, 2017, 9-17.
27. C. Cifuentes, M. Botero, E. Romero, C. Calderon, G. Gordillo, *Brazilian journal of physics*. **36(3B)**, 1046 (2006).
28. D.K. Schroder, *Semiconductor Materials and Device Characterisation (2nd Edition)*, A Wiley – Interscience Publication, John Wiley and Sons, Inc., (1998).
29. B. L. Theraja, *Textbook of Electrical Technology*; S.C. Hard and Company Ltd, 243 (2007).
30. A. B. Khatibani, A. A. Ziabari, S. M. Rozati, Z. Bargbidi, G. Kiriakidis, *Characterisation and Gas sensing performance of Spray Pyrolysed In₂O₃ Thin Films: Substrate Temperature effect*. *Transactions on electrical and Electronic materials*, **13(3)**, 111-115 (2012).
31. R. Davood, R. Taha, *The effect of heat treatment on the physical properties of Sol-gel derived ZnO Thin Films*, *Applied Surface Science*, **255**, 5812-5817 (2009).
32. Olivia, A. I., Maldonado, R. D., Diaz, E. A. and Montolvo, A. I. (2013). *A high absorbance material for solar collector's applications*, *Materials Science and Engineering*, **45**, 1-4.
33. A. F.M. Kamran, *Effect of Sol Concentration on Structural and Optical Behavior of ZnO Thin Films Prepared by Sol-gel Spin Coating*, *International Journal of Applied Physics and Mathematics*, **2 (6)** (2012).
34. N. Nagayasami, S. G. V. Veerasamy, *The Effect of ZnO Thin Films and Its Structural and Optical Properties Prepared By Sol-gel Spin Coating Method*, *Open Journal of Metal, Scientific Research* (2013).
35. M. Saleem, L. Fang, H. B. Ruan, F. Wu, Q. L. Huang, C. L. Xu dan C. Y. Kong, (2012). *Effect of zinc acetate concentration on the structural and optical properties of ZnO thin films deposited by Sol-Gel method* *International Journal of Physical Sciences*, **7 (23)**, 2971-2979.
36. C. Augustine, M.N. Nnabuchi, *Optical and solid state characterization of chemically deposited CuO/PbS double layer thin film*, *Materials Research Express*, **5(2)**, 1-11.
37. R.A. Chikwenze, and M.N. Nnabuchi, *Properties of lead selenide films deposited by chemical bath method*, *Chalcogenide Letters*, **7(5)**, 401-408 (2010).
38. P.N. Kalu, D.U. Onah, P.E. Agbo, C. Augustine, R.A. Chikwenze, and F.N.C. Anyaegbunam, and C.O. Dike, *The influence of deposition time and annealing temperature on the optical properties of chemically deposited cerium oxide thin films*, *Journal of Ovonic Research*, **14**, 293-305 (2018).
39. A.H.O. Al-khayatt, M.D. Jaafer, *Characteristics of nanocrystalline ZnS thin films grown on glass with different Zn ion concentrations by CBD technique*, **6(1)**, 27-35 (2014).
40. P.E. Agbo, P.A. Nwofe, L.O. Odo, *Analysis on Energy Band gap of zinc sulphide (ZnS) thin films grown by solution growth technique*, *Chalcogenide Letters*, **14(8)**, 357-368 (2017).
41. L. Kong, J. Deng, L.Chen, *Structural and optical characterization of magnetic sputtered ZnS thin films annealed in different atmosphere*, *Chalcogenide Letters*, **14(3)**, 87-96 (2017).
42. P. E. Agbo, M. N. Nnabuchi, D. U. Onah, *TiO₂ /Fe₂O₃ Core-shell Thin Film for application*, *Journal of Ovonic Research*, **7 (2)**, 29-35 (2011).
43. A. R. Chikwenze, *Solution growth and characterization binary selenide thin films for device applications*, *Ph.D Thesis, Department of Industrial Physics, Ebonyi State University, Abakaliki*, 305-338 (2012).
44. G. Nabiyouni, R Sahraei, M. toghiany, M. majies Ara, K. Hedayati, *Rev. Adv. Mater.Sc.*, **27**, 62 (2011).
45. W. Rika, H. Hardhienata, *IOP Conference Series: Earth and Environmental Science*, **54(1)**, 012094 (2017).
46. K.L. Chopra, P.D. Paulson, V. Dutta, *Thin film solar cells: an overview*, *Prog Photovolt: Research Applications*, **12**, 69-92.
47. K. Petkov, R. Todorov, D. Kozhuharova, I. Tcky, E. Cernoskova, P.J.S. Ewen, *J. Mat. Sci.* **39**, 961 (2006).
48. V. Bilgin, S. Kose, F. Atay, I. Akyuz, *The effect of substrate temperature on the structural and some physical properties of ultrasonically sprayed CdS films*, *Mater. Chem. Phys* **94**, 103–108 (2005).
49. Y. Natsume, H. Sakata, T. Hirayama, *Low temperature electrical conductivity and optical absorption edge of ZnO films prepared by chemical vapor deposition*, *Phys Stat Sol (A)* **148**, 485–95 (1995).

50. *S.J. Ikhmayies, R.N. Ahmad-Bitar, A study of the optical band gap energy and urbach tail of spray-deposited CdS:In thin films, Journal of Materials Research and Technology, 2(3), 221-227 (2013).*